Chapter 5

Digital Optical Switches with a Silicon-on-Insulator Waveguide Corner

DeGui Sun

Additional information is available at the end of the chapter

http://dx.doi.org/10.5772/intechopen.76584

Abstract

In this chapter, the quantum process of the Goos-Hänchen (GH) spatial shift is first derived out, then the coherence between spatial and angular shifts in the GH effect in the quantum state is discovered and a function of digital optical switch is developed. It is found that a waveguide corner structure always makes the reflected guide-mode have both the GH spatial and angular shifts when the incident beam is in the vicinity area of critical and Brewster angles. Meanwhile, these two GH shifts have the interesting coherent distributions with the incident angle, and only in the common linear response area the two GH shifts are mutual enhancing, then a mini refractive index modulation (RIM) of guided mode at the reflecting interface can create a great stable jump of reflected beam displacement at an eigenstate. As a result, on 220 nm silicon-on-insulator (SOI) waveguide platform, with a tapered multimode interference (MMI) waveguide a $5.0 \times 10^{18}\, cm^{-3}$ concentration variation of free carriers can cause a digital total 8–25 μm displacement of the reflected beam on the MMI output end, leading to a $1 \times N$ scale digital optical switching function. As a series of verifications, the numerical calculations, finite difference time domain (FDTD) simulations and experiments, are sustainable to the quantum GH shifts.

Keywords: silicon photonics, silicon-on-insulator, waveguide corner, coherent Goos-Hänchen spatial and angular shifts, eigenstate of total GH displacement, and digital optical switch

1. Introduction

In 1947 a novel spatial shift phenomenon of the reflected beam at an interface of two media was discovered by Goos and Hänchen, which was later referred to as the Goos-Hänchen (GH) effect [1]. Then, in 1948 it was theoretically modeled by V. K. Artmann by providing an

Artmann equation [2]. But, at that time no special attention was ever paid to this interesting phenomenon until 1972 when Chiu and Quinn further testified the simple delay process of optical scattering caused by this optical GH effect because Chiu and Quinn's work exactly presented the two polarization-determined parallel reflected beams in both theory and experiment [3]. In the past decades, based on the different media and technologies a variety of GH shift phenomena were studied in which their essential applications have been shown out [4–8]. At the condition of plane waves, the first impressive research in theory was done by Wild and Giles in [4]. Later, in 1986 Lai's team performed the more detailed theoretical investigation for the GH effect with Gaussian beam and obtained the more sustainable results, and furthermore in 2002 they extended their research to the more regular case—the complex expression for both the positive and negative electromagnetic materials at the reflection beam side and the frustrated total internal reflection (FTIR) was defined [5, 6]. These typical theoretical achievements in both plane and Gaussian waves have built a powerful fundamental for research on the GH behaviors of guided modes in a waveguide corner. Thus, in the past years, the establishments in the following three interesting topics relating to the GH effect have stimulated intensive research on new theories, materials and functionalities: (i) the integrated optical technologies due to a broad landscape of applications; (ii) the great spatial and angular shifts of Gaussian and quasi-Gaussian beams; and (iii) the control of GH effect in a micro-cavity by using the coherent light into the atomic energy levels [7–11]. With the special waveguide structures and corner-mirror materials, some novel phenomena of GH effect and the other involved effect such as Imbert-Fedorov shifts were also investigated and established [12–14].

In fact, the quantum mechanism supporting to theoretical research in the spatial shift of GH effect was established by Steinberg and Chiao in [15]. Then, in 2013 we theoretically demonstrated this quantum effect of the GH spatial shift with the consistent solutions of Maxwell equation and Schrödinger equation, and then proposed a digital electro-optic (EO) switching regime on semiconductor platform where a new metal-oxide-semiconductor (MOS)-capacitor type EO modulation method is also proposed and analyzed to realize an effective free-carrier dispersion (FCD) effect based refractive index modulation (RIM) [16]. Meanwhile, as a typical EO modulation scheme of semiconductor material, the FCD-based RIM of silicon-on-insulator (SOI) waveguide has been attracting the broad and intensive research attentions in the field of photonic integrated circuit (PIC) components and applications in the past decade [17, 18]. The similar part of all these FCD-RIM based switching schemes is that the FCD effect is imposed to a section of waveguide channel to cause an optical phase change, so their common intrinsic drawback is the FCD-induced optical absorption. As a result, there have not been any real accomplishments of product development reported so far. Consequently, the digital operations for the high-speed optical switching devices with advanced FCD-RIM schemes and device structures are expected for high-speed PIC devices [16–19].

In this chapter, by starting with the eigenstates of guided modes we first investigate the correspondences between the Fresnel equation and Schrödinger equation of guided modes and the coherence of the spatial shift and angular shift of the reflected guided modes under the GH effect. Then, the quantum processes responding to an incident angle with the eigenstates of guided modes of the MMI waveguide are discussed. Furthermore, the total displacement versus the concentration change of free-carrier holes is analyzed to discuss the performance

of FCD-RIM based digital optical switch within the SOI-CMOS submicron waveguide corner structure. Furthermore, the sustainable numerical calculations, professional software simulations and experiments are discussed. Finally, the conclusions are given.

2. Spatial and angular shifts in Goos-Hänchen (GH) effect

2.1. Coherence between the spatial and angular shifts in GH effect

Figure 1 shows the schematic relationship of incident, reflected and transmitted beams across the interface of two optical media with the refractive indices n_1 and n_2, respectively. A common definition of GH shift is the effective spatial shift Δ of the reflected beam axis at the direction perpendicular to the propagating direction of the reflected beam with respect to the ideal position, which can be forwarded to the expression of the displacement S_p along the reflective interface with the Artmann equation form as [2, 5, 15].

$$S_p = -\frac{d\phi}{k_1 \cos\theta d\theta} \tag{1}$$

where n_1 and n_2 stand for the refractive indices of the media at the reflected and transmitted sides, respectively, ϕ is the phase of the reflection coefficient ($r = R \cdot \exp(i\phi)$) if R indicates the amplitude coefficient), k_1 is the wave number ($k_1 = 2\pi n_1/\lambda_0$) if λ_0 is the optical wavelength in air, and θ and θ_t are the incident and transmitted angles of optical beam, respectively. In addition, an angular shift Θ is also caused under this GH effect.

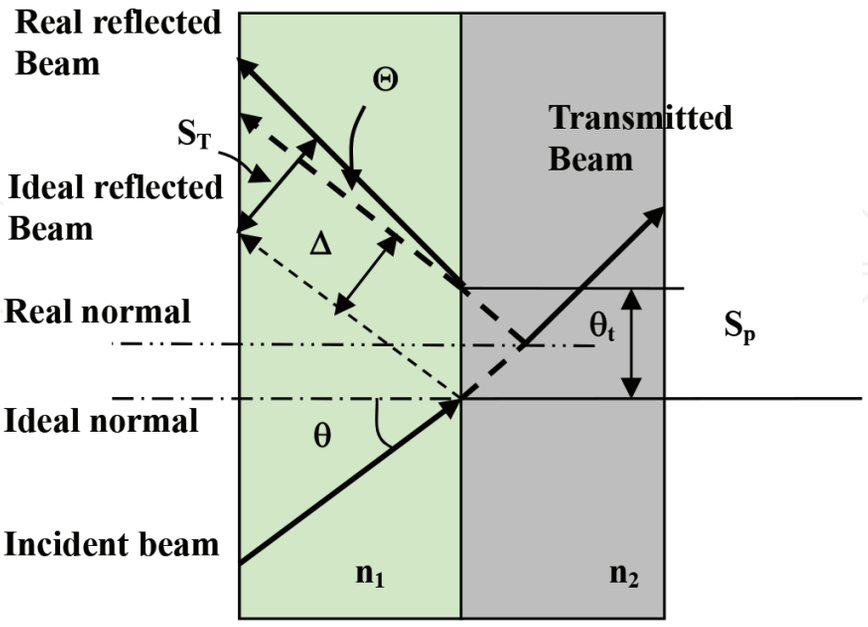

Figure 1. Schematic relationship of the incident, the reflected and the transmitted light waves at the interface of two optical media and the concepts of both GH spatial and angular shifts.

Eq. (1) tells that the phase change of reflected beam is a key parameter in the GH spatial shift, and this GH spatial shift must involve with a time delay no matter it is the light-wave traveling process of classical physics or the quantum mechanics. As demonstrated below, the optical phase change with incident angle is theoretically demonstrated to be either a quantum photonic process or the classical lightwave traveling mechanism, which is controlled by the delay time of the photon beam tunneling process in penetration depth [15, 16]. We know, in quantum mechanics theory, an electron beam in semiconductors can have a quantum-mechanical electron-wave transportation process to a potential barrier, so similarly a photon beam can also have a quantum-mechanical light-wave transportation process to a photon tunneling with a quantum effect. In 1990s, Steinberg and Chiao of the UC Berkeley did an experiment of passing through and blocking back of photon particles by using an optical system of two prisms with an air gas, then they found that the delay time of transmitted beam is shorter than the value calculated by the ray optical trajectory method, which is also referred to as an FTIR phenomenon. The FTIR phenomenon produces a quantum change of optical phase and was equivalently depicted as in **Figure 2**, where θ, θ_r and θ_t are the incident, reflected and transmitted angles of photon beam. If ϕ_d and τ_d are the phase change and the delay time of transmitted beam, respectively, after passing the penetration region of d, the transverse displacement Δz is expressed by [15].

$$\Delta z = -\frac{c}{n_1 \omega \cos\theta} \cdot \left[\frac{\partial \phi_d}{\partial \theta}\right]_\omega \tag{2}$$

where $\omega = 2\pi c/\lambda_0$ is the angular frequency of light-wave.

If we use ϕ replace ϕ_d in Eq. (2) to express the phase change in the penetration region of d, we immediately have solution as: $\Delta z = S_p$. We know, Eq. (2) is derived based on the electromagnetic formulism of quantum-mechanical electron-wave propagation from the Schrodinger

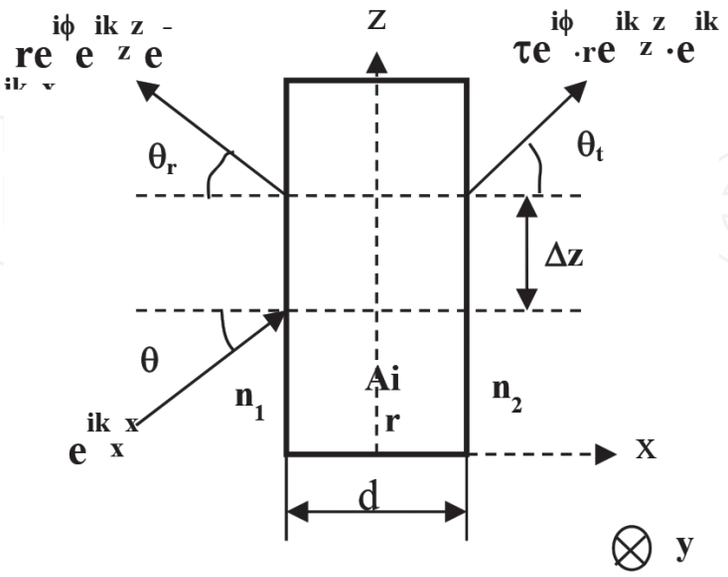

Figure 2. Schematic distribution of the one-dimensional phase shift due to the transverse displacement Δz when a photon beam tunnels a barrier with d thickness.

equation to define the transverse displacement Δz of both transmitted and reflected waves but it is the completely equivalent to the GH shift S_p defined by Eq. (1) that is evolved from the Maxwell equation of photon-wave. Thus, it turns out that the definition of the GH shift used in this work is very believable.

From Ref. [15], as shown in **Figure 2**, we have the delay time of transmitted beam during producing the shift Δz at the vertical direction as

$$\tau_d = \left[\frac{\partial \phi_d}{\partial \theta}\right]_\omega + \frac{n_2}{c}\Delta z sin\theta \tag{3}$$

Then, by comparing **Figure 2** with **Figure 1**, the delay time in Eq. (3) can be understood as the phase change of the reflected beam after it suffers from a GH shift. Then, setting $\Delta z/c = \tau_d$ yields

$$\frac{\Delta z}{c} = \left[\frac{\partial \phi_d}{\partial \theta}\right]_\omega + \frac{\Delta z}{c} n_2 sin\theta \tag{4}$$

Substituting Eq. (2) into Eq. (4) yields

$$-\frac{1}{n_1 \omega cos\theta} \cdot \left[\frac{\partial \phi_d}{\partial \theta}\right]_\omega = \left[\frac{\partial \phi_d}{\partial \theta}\right]_\omega - \frac{n_2 sin\theta}{n_1 \omega cos\theta} \cdot \left[\frac{\partial \phi_d}{\partial \theta}\right]_\omega \tag{5}$$

Then, we obtain

$$\left[\frac{1 + n_1 \omega cos\theta - n_2 sin\theta}{n_1 \omega cos\theta}\right] \cdot \left[\frac{\partial \phi_d}{\partial \theta}\right]_\omega = 0 \tag{6}$$

We know θ is an angle close to the Brewster angle or the critical angle of the optical TIR system shown in **Figure 1** and $n_1 \omega cos\theta \gg n_2 sin\theta$, so we have the final solutions as

$$\frac{1 + n_1 \omega cos\theta - n_2 sin\theta}{n_1 \omega cos\theta} \neq 0 \text{ and } \left[\frac{\partial \phi_d}{\partial \theta}\right]_\omega = 0 \tag{7}$$

Thus, the term $\left[\frac{\partial \phi_d}{\partial \theta}\right]_\omega$ must be the critical values of the function ϕ_d with respect to θ, i.e., $\phi_d(\theta)$.

2.2. Duality of spatial and angular shifts in GH effect

In 1980s the scientists of the United States predicted, it is reasonable for the reflected beam to display a small angular deviation from the law of specular reflection [20, 21]. Until two decades later, in 2006 and 2009, the experimental results of the angular shift under the GH effect were observed in microwave and optical domains, respectively [9, 22]. In the optical experiments, the general role of GH spatial and angular shifts is modeled with both the phase and amplitude of reflected beam, then with **Figure 1**, by setting a multimode interference (MMI) with l_{mm} length, the total beam displacement is defined by a combination of the spatial shift Δ and angular shift Θ as [22]

$$S_T = \frac{1}{\cos\theta}(\Delta + l_{mm}\Theta) \tag{8}$$

where l_{mm} stands for the length of tapered reflective MMI waveguide. From the reflection coefficient $r = R \cdot \exp(i\phi)$, the general algebra expression of the GH shift can be expressed as

$$D = \frac{\partial \ln r}{\partial \theta} = \frac{1}{R}\frac{\partial R}{\partial \theta} + i\frac{\partial \varphi}{\partial \theta} \tag{9}$$

Then, with the propagation constant of the input guided mode β_{in}, the combination of Eqs. (8) and (9) yields the spatial and angular shifts in the GH effect as

$$\Delta = \frac{1}{\beta_{in}}\frac{\partial \varphi}{\partial \theta} = \mathrm{Im}(\ln r) \tag{10a}$$

$$\Theta = \frac{2}{(\beta_{in}^2 w_0^2)}\frac{\partial R}{\partial \theta} = \mathrm{Re}(\ln r) \tag{10b}$$

where w_0 stands for the waist of an approximated Gaussian beam of reflected guided mode. Therefore, in terms of the set of Eqs. (10a) and (10b), the GH spatial and angular shifts involve with the phase and amplitude of the reflected beam, respectively.

For the TE- and TM-mode, the amplitude reflection coefficients R_{TE} and R_{TM} are, respectively, defined by [6, 16]:

$$R_{TE} = \frac{\cos\theta - (\eta^2 - \sin^2\theta)^{1/2}}{\cos\theta + (\eta^2 - \sin^2\theta)^{1/2}} \tag{11a}$$

$$R_{TM} = \frac{\eta^2\cos\theta - (\eta^2 - \sin^2\theta)^{1/2}}{\eta^2\cos\theta + (\eta^2 - \sin^2\theta)^{1/2}} \tag{11b}$$

where $\eta = N_{eff}/n_m$ when N_{eff} is the effective refractive index of the guide mode of input waveguide and n_m is the refractive index of corner mirror material. In Ref. [16], for the eigenstate of reflected mode on the GH spatial shift, the partial derivative meets $\partial\phi/\partial\theta = 0$, so the incident angle θ must have its corresponding eigenvalue, which creates a critical value of wave function $\varphi(x, y, z)$. From Eqs. (10b) and (11) we find that the GH angular shift Θ is dependent of the effective index N_{eff}, while N_{eff} is determined by the input waveguide material.

2.3. Understanding to the quantum spatial and angular shifts in GH effect

We know all the guided modes of an MMI waveguide are the eigenstates of quantum physical process and the corresponding effective indices are the eigenvalues of all the refractive indices of optical beam at the phase velocities [23, 24]. So, if we set the input waveguide channel as a single-mode, N_{eff} would be only the eigenvalue of the single-mode, then it finally determines one of the GH angular shifts. Thus, for a waveguide structure, if $\varepsilon_r(x)$ stands for the relative

dielectric constant of waveguide material, the two-dimensional (2D) Maxwell wave equation of the propagation constant β and light wave function $\varphi(x, z)$ for the TE- and TM-mode of optical waveguide are expressed by (12a) and (12b), respectively, as [25].

$$2j\beta \frac{\partial \varphi(x, z)}{\partial z} = \frac{\partial^2 \varphi(x, z)}{\partial x^2} + k_0^2\left(\varepsilon_r^2 - N_{eff}^2\right)\varphi(x, z) \tag{12a}$$

$$2j\beta \frac{\partial \varphi(x, z)}{\partial z} = \varepsilon_r \frac{1}{\partial x}\left(\frac{1}{\varepsilon_r}\frac{\partial \varphi(x, z)}{\partial x}\right) + k_0^2\left(\varepsilon_r^2 - N_{eff}^2\right)\varphi(x, z) \tag{12b}$$

For a quantum system, if $U(x)$ and $m(x)$ stand for the arbitrary potential and the effective mass, respectively, with the effective mass approximation and the Plank constant $\hbar$, the time-dependent relation for the photon wave function $\Psi(x, t)$ can be expressed by a Schrödinger equation as

$$j\hbar \frac{\partial \Psi(x, t)}{\partial t} = \frac{\hbar^2}{2}\frac{\partial}{\partial x}\left(\frac{1}{m(x)}\frac{\partial \Psi(x, t)}{\partial x}\right) + U(x)\Psi(x, t) \tag{13}$$

Comparing (13) with (12a) and (12b) yields the conclusions that the TE-mode corresponds to the case that the effective mass is independent of x, while the TM-mode corresponds to the case that the effective mass is dependent of x. Hence, we can find the following correspondences for qth mode:

$$z \leftrightarrow t, \tag{14a}$$

$$2j\beta \leftrightarrow j\hbar, \tag{14b}$$

$$\frac{\partial^2}{\partial x^2} \leftrightarrow \frac{\hbar^2}{2m}\frac{\partial^2}{\partial x^2} \text{ for TE-mode} \tag{15a}$$

$$\varepsilon_r \frac{1}{\partial x}\left(\frac{1}{\varepsilon_r}\frac{\partial}{\partial x}\right) \leftrightarrow \frac{\hbar^2}{2}\frac{\partial}{\partial x}\left(\frac{1}{m(x)}\frac{\partial \Psi(x, t)}{\partial x}\right) \text{ for TM-mode} \tag{15b}$$

$$k_0^2\left(\varepsilon_r^2 - N_{eff}^2\right)\varphi(x, z) \leftrightarrow U(x)\Psi(x, t) \tag{16}$$

It turns out that the angular shift defined by Eq. (10b) is a quantum selection from multiple eigenstates of the reflection angle under the GH effect. It turns out from relation (14a) that the distance z of light wave traveling corresponds to the time t of photon beam tunneling, while in quantum mechanism, there is no variation of particle velocity, so this corresponding relation is very reasonable. It turns out from relation (14b) again that the propagation constant relates the effective wave number of the guided mode in the traveling-through channel, while the Plank constant $\hbar$ relates the eigenstate of particle with its mass in tunneling barrier, so the guided mode is limited to a quantum state. Therefore, the relations, (15a), (15b) and (16) are used to analyze the field-distributions of guided mode at its eigenstate.

3. A digital optical switch principle with the waveguide corner

3.1. Device concept and condition for the digital optical switch

With the SOI-based waveguide corner mirror (WCM) structure comprising semiconductor (silicon) waveguide channel material, oxide (SiO_2 or SiON) corner mirror material and metal material for electrodes, a new regime of 1xN scale digital optical switches was proposed as shown in **Figure 3**. This special regime of digital optical switches composed of a single-mode input waveguide, a tapered multi-mode corner waveguide, a corner mirror and N single-mode output waveguides is proposed, where N is an integer. In this device regime, the single-mode output waveguide channels are all in conjunction with the output end of the tapered MMI corner waveguide [15, 16]. Then, the free-carrier concentration variation at the interface area of mirror and waveguide is controlled to realize the FCD-RIM of silicon of this WCM structure [16–19].

In optical switching operations, as shown in **Figure 3**, all the possible angles of the reflected guided mode are no longer the same due to an angular shift of the GH effect. Namely, the angular shift in this project makes the reflection angle different from the input angle and then creates a great total displacement at the output end of tapered MMI waveguide with a combined effect of the spatial shift and angular shift as defined by Eq. (8).

3.2. Discussion for the mode distributions of MMI waveguide

In this 1xN type digital EO switch shown in **Figure 3**, the tapered MMI waveguide is a critical part as it not only forms a reflecting interface with the corner mirror, but also transfers the reflected optical beam from a single-mode input waveguide to its corresponding single-mode output waveguide. Thus, at the input end this tapered MMI waveguide is required not only to have the corresponding eigenstate guided mode to match the eigenstate reflected-mode of the GH effect, but also have the length to maintain the single-mode state of reflected guided mode from the input waveguide to the corresponding output waveguide.

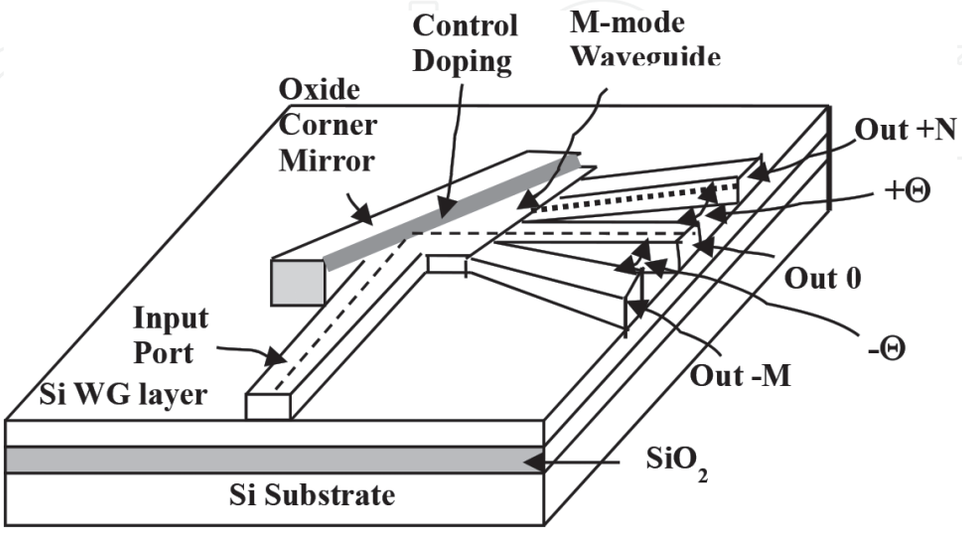

Figure 3. Schematic architecture of the SOI-WCM for the GH effect based 1x3 optical switch with CMOS-compatible sub-micron scale waveguides and FCD-RIM.

With the consideration for both the GH spatial and angular shifts in the FTIR process of WCM structure, the tapered MMI waveguide was set to meet the conditions at its input end so that it can produce a sufficient separation between two adjacent output modes at its output end. As explained above, the tapered MMI waveguide is assumed to contain N modes with the numbers q = 0, 1, …, N-1, the GH angular shift defined by Eq. (10b) is a quantum selection for the eigenstate reflection angle of a reflected guide-mode to match one of the multiple guided modes of tapered MMI waveguide at its input end which has an effective index N_{eff}. **Figure 4** schematically depicts such a tapered MMI waveguide where W_i and W_0 are its widths at the input and output ends, respectively, and the total displacement S_T is determined by the spatial and angular shifts as defined by Eq. (8).

In the MMI waveguide a specified factor is the beat length of the two lowest-order modes (i.e., the two key modes) L_π, which is defined by the propagation constant difference of these two modes $\Delta\beta_{01} = \beta_0 - \beta_1$ as

$$L_\pi = \frac{\pi}{\Delta\beta_{01}} \approx \frac{4 n_1 W_i^2}{3\lambda_0} \tag{17}$$

The 1-mode length is required to be $L_{1m} = \left(\frac{3}{4}\right) L_\pi$, then we have:

$$L_{1m} = \left(\frac{3}{4}\right) L_\pi \approx \frac{n_1 W_i^2}{\lambda_0} \tag{18}$$

For the qth mode eigenstate guided mode, the lateral wavenumber k_{kq} and the propagation constant β_q should be related to a core refractive index n_1 of waveguide as [23, 24]

$$k_{xq}^2 + \beta_q^2 = k_0^2 n_i^2 \text{ with} \tag{19a}$$

$$k_0 = 2\pi/\lambda_0, k_{kq} = (q+1)\pi/W_i \tag{19b}$$

Accordingly, the propagation constant spacing of any high order mode from the fundamental mode is expressed as

$$\Delta\beta_{0q} = \beta_0 - \beta_q \approx \frac{q(q+2)\pi}{3 L_\pi} \tag{20}$$

3.3. Matching condition between the RIM modulation and the guided mode

In the FCD-RIM process of an SOI-waveguide device, if the concentration of free-carriers in silicon waveguide has a variation for the guided mode, at λ = 1550 nm the RIM of silicon is defined by the refined Drude-Lorentz model as [18, 19].

$$\Delta n = -\left[8.8 \times 10^{-22} \Delta N_e + 8.5 \times 10^{-18} (\Delta N_h)^{0.8}\right] \tag{21a}$$

$$\Delta\alpha = 8.5 \times 10^{-18} \Delta N_e + 6.0 \times 10^{-18} \Delta N_h \tag{21b}$$

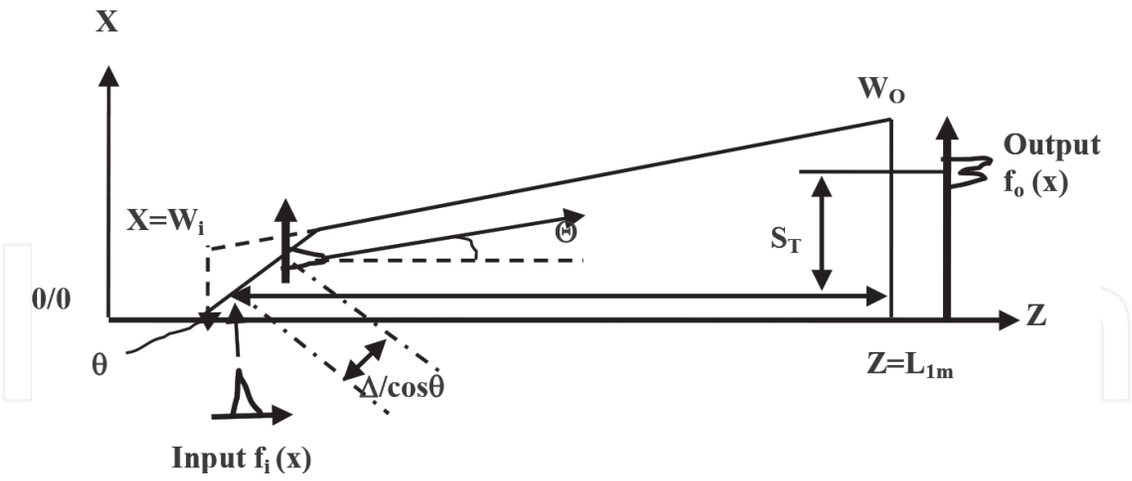

Figure 4. Schematic structure of the tapered MMI corner waveguide for transferring the reflected optical beam from the input waveguide to an output waveguide at the single-mode state with 1-mode length $Z = L_{1m}$, where the spatial/angular shifts, and the total displacement of GH effect are labeled.

where Δn and $\Delta\alpha$ are the changes of refractive index and absorptive coefficient, respectively, resulting from the variation in free carrier concentrations; ΔN_e and ΔN_h are the concentration variations of free electrons and free holes, respectively. Eqs. (21a) and (21b) imply that the FCD-RIM effect also causes an extra optical loss in its refractive index modulation. For the reflection of the guided mode at the waveguide/corner-mirror interface, the incident and reflected optical fields should be expressed as [26, 27].

$$E_i = \exp.[i(\omega t - k_i z)] \text{ and } E_r = R \cdot \exp[i(\omega t - k_r z)] \tag{22}$$

where the reflection coefficient R is defined by Eqs. (11a) and (11b) for TE- and TM-mode, respectively. Finally, at the qth independent mode in the FTIR process from the input mode to the reflected mode, we have a transmission equation of Fresnel formula between the critical angle θ_C and the effective index N_{eq} as.

$$n_2 \approx N_{eq} \sin[\theta_C + \Theta_q] \tag{23}$$

We know, there are more than two guided modes in the input end of an MMI waveguide and any independent guided mode has an independent N_{eq} value [23, 24], so it is the exclusive value to determine a jump of the reflected beam in this GH effect.

4. Simulations and analyses for the FCD-based modulation performance

In Section 2.2, we theoretically have proved that both the GH spatial and angular shifts form a total displacement of reflected beam at the output end of MMI waveguide. So, the performance of this digital optical switch is based on the dual GH shifts.

4.1. Analysis for both the spatial and angular shifts of GH effect

By selecting the CMOS-compatible SOI waveguide and taking the silicon layer thickness as H = 220 nm, ridge height as h = 130 nm, silicon refractive index as n_1 = 3.43, and SiO_2 refractive index as n_2 = 1.46, then for the rib widths: 350 and 400 nm, with the finite-difference time-domain (FDTD) software we obtain the effective indices and the corresponding effective widths of the guided modes at λ=1550 nm and x-polarization as depicted in **Table 1**.

As shown in **Figures 3** and **4**, the GH effect happening on the FTIR interface has the changes of two physical parameters—the position and angle of reflected beam, which both strongly depend on the incident angle θ when it is close to the Brewster critical angle θ_C. As depicted in **Table 1**, the rib widths of 350 and 400 nm have the effective indices as N_{eff} = 2.3368 and N_{eff} = 2.4114, respectively, which lead to the critical angles as θ_C = 38.7 and 37.3°, respectively. Hence, for these two rib widths with the theoretical models defined by Eq. (10a) we first display the dependences of the GH spatial shift Δ on the incident angle θ of optical guided mode as shown in **Figures 5(a)** and **5(b)**, respectively. Note from **Figure 5** that a sharp change can be caused by a mini-change of incident angle at a vicinity of the Brewster critical angle θ_C, and the GH spatial shifts are different between the two different cases of incident angle: smaller and greater than θ_C.

In our previous work, the switching scale potential of digital optical switch scheme was only based on the GH spatial shift. However, as analyzed above, in a real FTIR process the reflected beam not only has an anti-trajectory rule phenomenon of reflecting position, but it also predicts a non-specular reflective angle shift, thus as a continuous research project, these two special photonic phenomena in the FTIR process are both dependent on one quantum state of photonic tunneling process. In the same manner, when the input single-mode waveguide has the rib widths of 350 and 400 nm, with the data used for **Figure 5** and Eq. (10b) we further obtain the simulations for the dependences of the GH angular shift Θ of reflected mode on the incident angle θ as shown in **Figures 6(a)** and **6(b)**, respectively. Note from **Figures 5** and **6** that, under the quantum GH effect, both the spatial and angular shifts of reflected beam have the sharp responses to the incident angle and are mutually influenced. However, the difference between these two shifts is that the spatial shift Δ is plus while the angular shift Θ is minus, which can be manipulated to realize a switching function with the WCM structure.

By selecting the rib width of 350 nm, the dual dependences of spatial and angular shifts on the incident angle is shown in **Figure 7**. Two significant interesting points should be found in **Figure 7** as that (1) in a vicinity of Brewster critical angle θ_c that is at 38.95°, the incident angle greater than θ_c must be selected where the angular shift is extremely big at the minus direction and (2) the two GH shifts have one common sharp linear response range. In **Figure 6**, there are five different areas in the whole distribution of the two GH shifts as: (1) In the area of incident angle smaller than 38.5° only a slow angular shift exists; (2) in the area of incident angle from 38.5 to 38.91° the two GH shifts are reverse; (3) in the area of incident angle from 38.91 to 38.95°, the two GH shifts have a common linear response area; (4) in the area of incident angle from 38.96 to 39.30° that is exactly greater than θ_C the two GH shifts are reverse again; and (5) in the area of incident angle greater than 39.3° only a slow spatial shift exists. In the common linear response area of these two GH shifts we find that at the incident angle of 38.91°, the spatial GH shift reaches its minimum value of 3.82 μm, while the GH angular

Rib width, W_r (nm)	350	400
Effective index at E_x, N_{eff}	2.3368	2.4114
Effective mode-width at E_x, W_{eff} (nm)	~350	~400

Table 1. Single-mode operations of two rib widths.

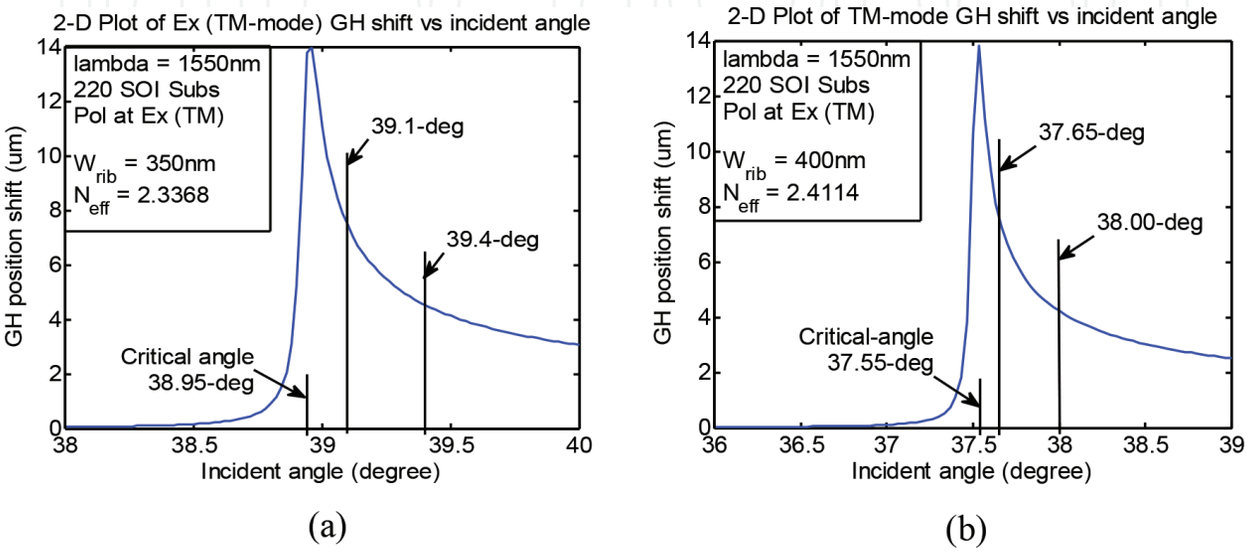

Figure 5. Incident angle dependence of the spatial shift of reflected beam under the GH effect with the WCM structure at the x-polarization: (a) and (b) are for 350 and 400 nm rib widths, respectively, where the typical values of incident angle are marked.

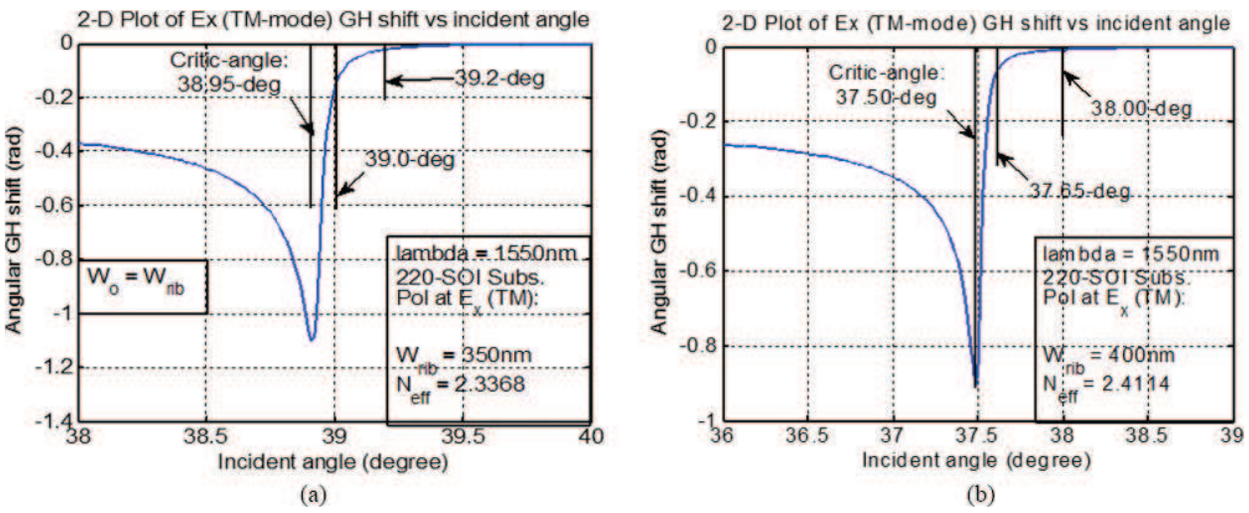

Figure 6. Incident angle dependence of angular shifts under the GH effect with the WCM structure at x-polarization: (a) and (b) are for 350 and 400 nm rib widths, respectively, where the typical values of incident angle are marked.

http://dx.doi.org/10.5772/intechopen.76584

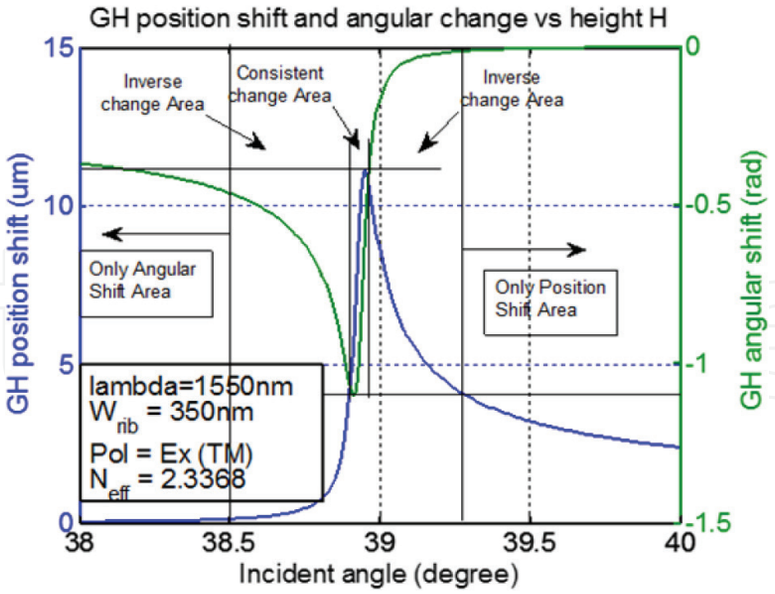

Figure 7. For the 350 nm rib width and at 1550 nm wavelength the incident angle dependences of both the spatial and angle shifts under the GH effect in which the characteristics of GH shifts are categorized.

shift reaches its maximum value of −1.10-rad. In contrary, when the incident angle is in the range of 38.94–38.95°, the GH spatial shift reaches its maximum value of 11.14 μm, while the GH angular shift reaches its lowest value of −0.35-rad. These characteristics of the common response area of GH shifts are very conducive to the designs of digital optical switches.

4.2. Analysis for the mode distribution at the input end of MMI waveguide

In order to meet the mature fabrication technique for future experiments, we select the CMOS-compatible 220 nm standard SOI-PIC platform with 130 nm rib height, at $\lambda = 1550$ nm the refractive indices for core and cladding layers are 3.43 and 1.46, respectively. For the input waveguide having a rib width of 350 nm, at the input end of MMI waveguide as shown in **Figure 8(a)**, we calculate the optical field distribution of reflected guided mode as depicted in **Figure 8(b)**. Note that the mode size is approximately 2.00 μm, so at the input end of the MMI waveguide the smallest center-center spacing between two adjacent ports is 2.00 μm, then total width should be set in the range from 2.00 to (2.00 + 11.4) μm.

4.3. Investigation for the total GH displacements at the MMI output end

In accordance with the simulations of both the spatial and angular shifts of GH effect shown in **Figures 5** and **6**, we determine the input end width $W_i = W_{eff} + \Delta$. As an illustration, by taking W_i as 2.5 μm, we calculate L_{1m} with Eq. (18) at first, and then with Eq. (8) obtain the total displacement S_T at the output end of the MMI waveguide in its linear response range to incident angle as shown in **Figure 9**.

Note from **Figure 9** that the sharp response range is the common linear response area of the two GH shifts in **Figure 6**, which is in the range of incident angle from 38.91 to 38.95° and

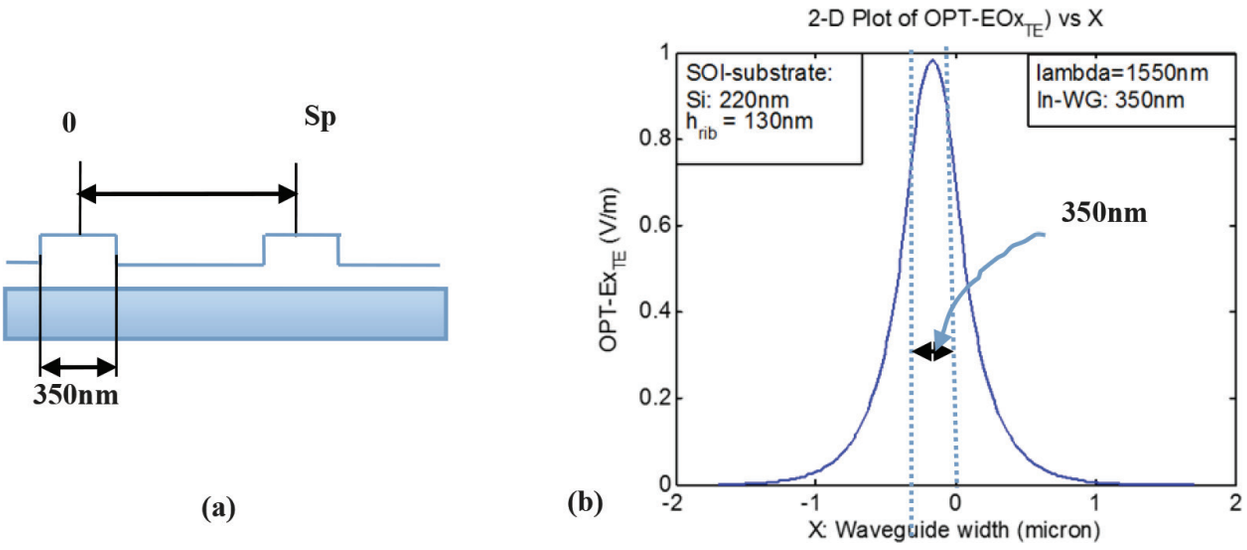

Figure 8. Optical field distribution of single-mode at the input end of MMI waveguide channel having a ridge width of 350 nm: (a) the input port cross-sectional view and (b) the optical field distribution.

labeled as a consistent change area, and in the other two incident angle areas, namely, it is smaller than 38.91° and greater than 38.96°, there are two the moderate response ranges of S_T to the incident angle. Such the distribution characteristics of the total displacement S_T at the output end of MMI waveguide are very conducive to the optimization of digital optical switch performance. Thus, it turns out that **Figure 9** is paramount important for investigating the maximum feasible switching scale and designing the best optical switch with the WCM structure and the FCD-RIM.

From **Figures 5** and **6** we know the sharp-response area of GH effect to the incident angle is a consistent area between the spatial shift and the angular shift under this GH effect, and **Figure 9** proves that the total displacement is co-contributed by the spatial and angular shifts. So, as a result, in the incident angle range from 38.83 to 39.16° it presents a sharp linear response area to the incident angle for a given MMI width at its input end. Therefore, for this 350 nm rib waveguide we first select the incident angles as 38.7, 38.9 and 39.1° in the sharp-response area of GH effect in **Figure 9** that are all very close to the critical angle and then at the wavelength of 1550 nm obtain the dependence of the total displacement of the reflected beam on the free-carry hole concentration change (HCC) for the two given MMI waveguide width values at its input end: 2.5 and 5.0 μm as shown in **Figure 10(a)** and **(b)**, respectively. In this process, as described above, the HCC activates an RIM of silicon material at the reflective interface between the silicon material of waveguide and the silicon-dioxide of corner mirror as defined by the Drude-Lorenz Eq. (21). In fact, **Figure 10** presents one significant attribute of the GH-effect based total displacement of reflected beam when the HCC is changed from 0 to $2.5 \times 10^{18}\, cm^{-3}$. Note that the displacement immediately passes through an unstable quantum jump and stabilizes on the values of −15 and −30 μm for the MMI widths of 2.5 and 5.0 μm, respectively, irrespective of the HCC continuous increasing. So, the quantum switching property has been shown out, but such a complex process will take much more research before realizing a digital optical switch.

http://dx.doi.org/10.5772/intechopen.76584

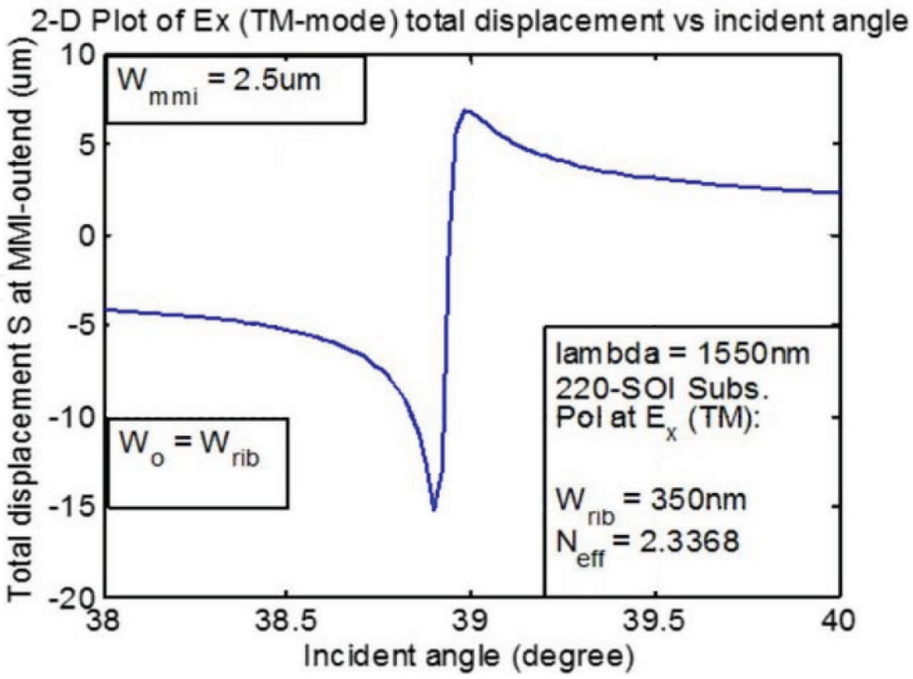

Figure 9. The total displacement at the interface of reflected beam for the rib width 350 and W_i = 2.5 μm at 1550 nm wavelength.

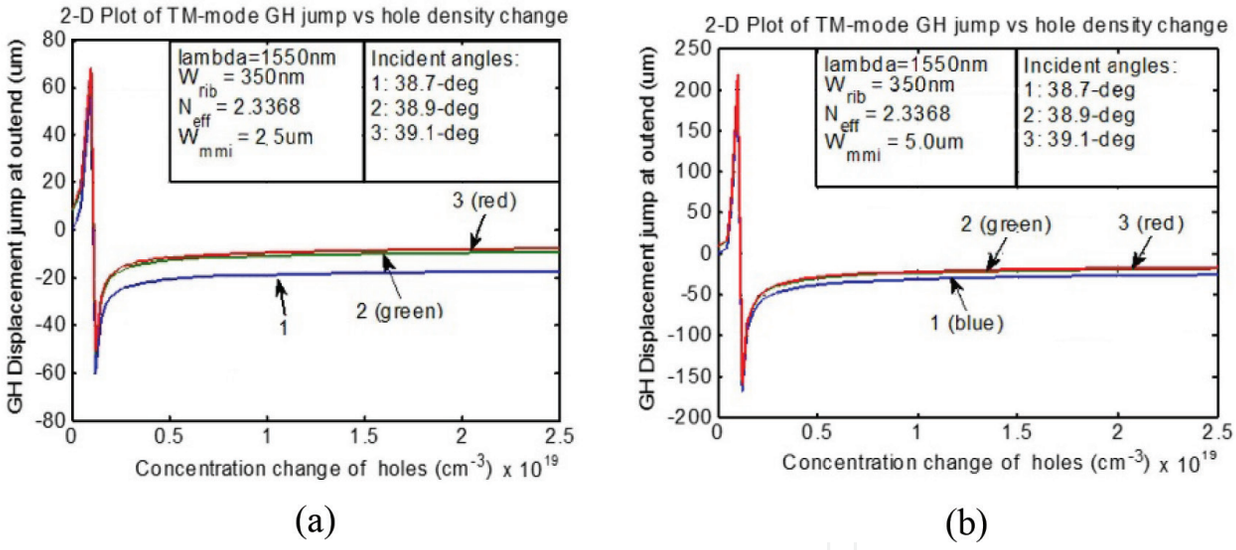

Figure 10. Dependence of the total space displacement of reflected guided mode caused by two GH shifts for the waveguide width of 350 nm at the sharp response area with respect to three different incident angles: (a) and (b) for the input end width of MMI waveguide: 2.5 and 5.0 μm, respectively.

Similarly, by selecting three incident angles: 39.1, 39.3 and 39.5° that are in the moderate area of **Figure 9** for the incident angle greater than the critical angle we obtain the total displacement dependence of the reflected beam on HCC as shown in **Figure 11** where (a) and (b) are still for the two MMI waveguide input-end widths: 2.5 and 5.0 μm, respectively. Note from **Figure 11** that the HCC of $5.0 \times 10^{18}\ cm^{-3}$ can cause the total displacement to have a stable quantum

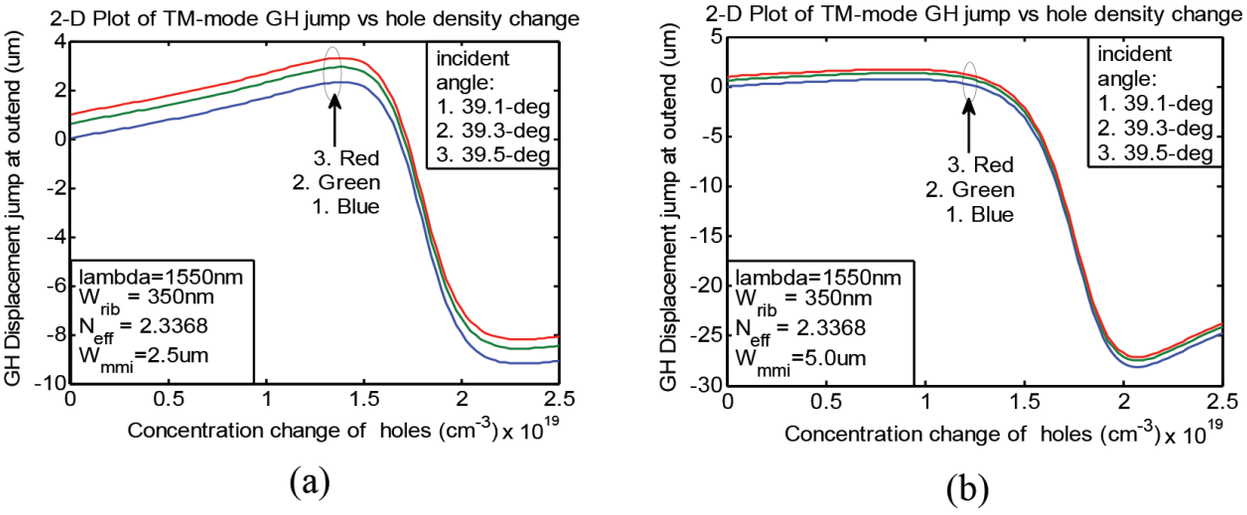

Figure 11. Dependence of the total displacement on the HCC under GH effect for waveguide width of 350 nm in the moderate response area with respect to three incident angles: (a) and (b) are for the input end widths of MMI waveguide: 2.5 and 5.0 μm, respectively.

jump, which is −8 and −25 μm for the MMI waveguide widths of 2.5 and 5.0 μm at the input end, respectively. Although the total displacements have the different jump amplitudes for these two MMI waveguide widths they need the same HCC value of $5.0 \times 10^{18}\, cm^{-3}$ to cause an FCD-RIM of about $6.0 \times 10^{18}\, cm^{-3}$ via Eq. (21). Hence, as a substantial application and one of the objectives of this work, a digital switching operation can be immediately convinced. With the free-carrier concentration control structure MOS-capacitor [16, 19], the HCC of $5.0 \times 10^{18}\, cm^{-3}$ can be controlled to be 3–5 stages by controlling both the gate and source voltages, then $1 \times N$ type digital optical switching function could be realized, where the scale metric N depends on the system design and the requirement for the isolation between any two outputs.

5. Verification for the GH shifts

5.1. Simulations for the GH spatial shift with finite difference time-domain (FDTD) software

As early as the end of 1990s, we had started to investigate the optical output performance of waveguide corner mirrors with the theoretical modeling, numerical and professional software simulations and published the achievements in 2009 [27]. Based on the numerical calculations and finite difference time-domain (FDTD) simulations for the optical power transfer efficiency of SOI waveguide corner mirrors, an SOI rib waveguide structure is designed as shown in **Figure 12(a)**, then in order to specially simulate the impact of the GH shift on the optical power transfer efficiency, a waveguide corner mirror (WCM) structure is designed to have one input single-mode waveguide channel and one output single-mode waveguide channel as shown in **Figure 12(b)**, where the reflecting mirror is created with a step fabrication of deep etching as shown in **Figure 12(c)**.

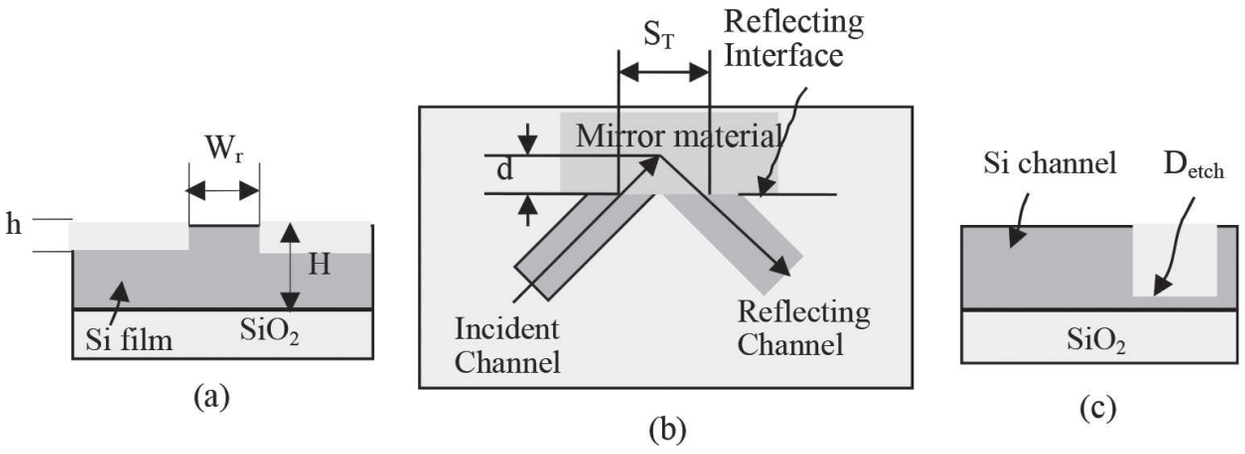

Figure 12. Schematic SOI rib waveguide corner mirror (WCM) structure: (a) the cross-sectional view of rib waveguide; (b) the distribution of waveguide channels and corner mirror with a GH shift d and (c) the deep etched part as corner.

In **Figure 12(b)** the position d is set to create a previous set GH spatial shift as: $S_T = -2d \cdot tan(\theta)$. With the feasible designs and fabrications of the real devices, two standards of SOI substrate: thick and thin silicon films are selected and the corresponding waveguide structures for each standard for single-mode operations are depicted in **Table 2**. Then, by setting the reflecting interface roughness as $\sigma = 100 - 500\,\mathring{A}$ and the tilt-angle as $\varphi = 0, 1, 2^{\circ}$, with the thick SOI standard and large-scale waveguide rib width of 4.0 μm, the numerical calculation as shown in **Figure 13(a)**. Note that both the position and tilt-angle of the reflecting interface play the significant impacts upon the optical power transfer efficiency. In the same manner, by selecting the roughness as $\sigma = 100\,\mathring{A}$ and the tilt-angle of reflecting interface as $\varphi = 0, 1^{\circ}$ with the thin SOI substrate listed in **Table 2**, the FDTD simulation results of the GH shift dependence of optical power transfer efficiency as shown in **Figure 13(b)**. One novel finding from **Figure 13(b)** is that the GH shift dependence curves of the optical power transfer efficiency of TE- and TM-mode have an intersection, which could never happen to any parameter dependence curves, so this novel phenomenon implies the discontinuous characteristics of the optical power transfer efficiency when the GH shift impacts the TIR process. In addition, the minus d value gives the highest optical power efficiency, matching the situation of the plus S_T value.

5.2. Design, fabrication and test of SOI waveguide corner mirror structure

We designed, fabricated and characterized the WCM structures in 2009-2011 and presented the achievements in 2013 [19]. Based on the fabrication condition of SOI waveguides, we

SOI substrate standard	Thick Si film, 4.0 μm	Thin Si film, 1.5 μm
Rib width, W_r (μm)	4.0	2.0
Rib height, h (μm)	1.0	0.5

Table 2. Two SOI standards and the corresponding rib widths for single-mode operations.

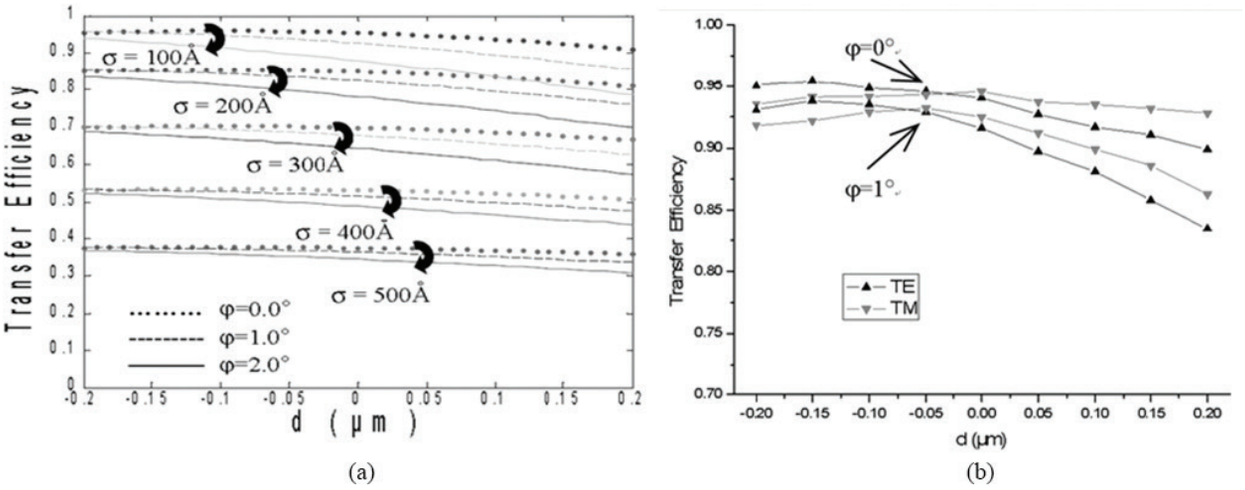

Figure 13. Dependence of optical output on the GH spatial shift GH effect for the thick SOI standard: (a) the numerical calculation results with the thick SOI substrate and (b) the FDTD simulations with the thin SOI substrate.

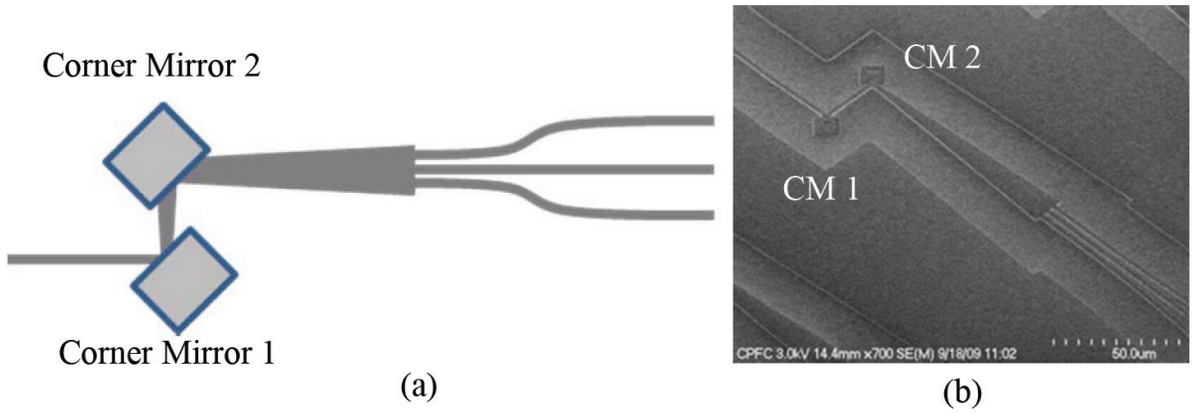

Figure 14. Design & fabrication of SOI-WCM having 1 input waveguide channel and 3 output waveguide channels: (a) the schematic layout of 1 × 3 SOI-WCM and (b) the perspective view SEM image of a fabricated device sample.

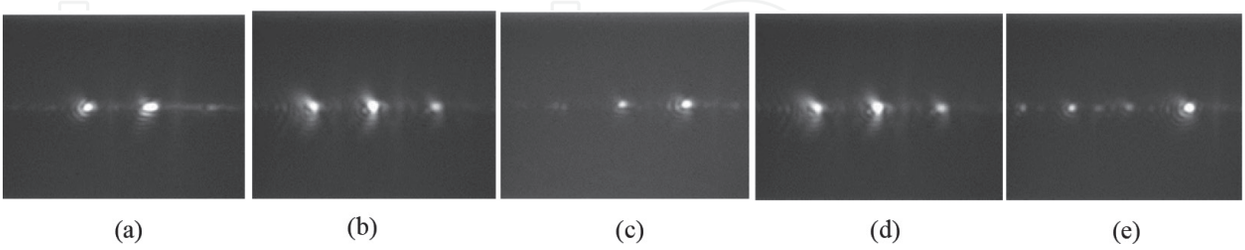

Figure 15. Testing results of optical outputs at three ports for the fabricated devices with five GH shift values that can be caused by FCD-based RIM with 2d of: (a) −0.3 μm; (b) −0.15 μm; (c) 0; (d) +0.15 μm; and (e) +0.30 μm.

selected the thin SOI substrate and then designed the 1 × 3 type WCM structure according to the regime of digital optical switches for evaluating the optical performance of both the GH shift effect and indirectly measuring the switching possibilities of digital optical switch as shown

in **Figure 14(a)** and then the SEM image of fabricated device sample is shown in **Figure 14(b)**. By setting 5 values of d as: -0.15, -0.07, 0, 0.07 and 0.15 μm on each corner, we obtained 5 optical output modes as shown in **Figure 15** from (a) through (e). A very significant point is that the two minus d values: −0.15 and −0.07 μm give the obvious higher optical output at the middle port than the case of $d = 0$, but there is no obvious difference between these two d values, which is probably due to the quantum effect of the two GH shifts apart from the non-uniformity of fabrication. For the two plus d values: 0.15 μm, the output at the right port is higher than the cases of both $d = 0$ and d = 0.07 μm due to GH effect.

6. Conclusions

In this chapter, based on the coherent quantum process of the GH spatial and angular shifts, the new mechanism of substantial digital optical switches is investigated with a WCM structure. For the new regime of digital optical switches, an ideal optical refractive index modulation is FCD effect of semiconductor silicon for ultrahigh speed switching operations of pico- and nanosecond levels, but the other refractive index modulation such as the thermos-optic modulation can also be selected to realize the μs level operations. In addition, the mutual enhancing contributions of the two quantum GH shifts can be further developed to optimize the total displacement of reflected beam for digital optical switches. Therefore, this work will be helpful for research and development of high integrable and high-speed optical and photonic switches on the platform of silicon photonics.

Acknowledgements

This work is co-sponsored by the Innovative R&D Fund of CUST/China, the Research Program of Ontario Centre for Excellences (OCE) /Canada, and the in-kind invest of D&T Photonics, a startup spun-off from University of Ottawa. Author is very grateful for Prof. Trevor J. Hall for his supervising in design and fabrication of the experimental samples, and also thanks his graduated students: Xiaoqi Li and Jia Yi for their supporting works.

Author details

DeGui Sun[1,2]*

*Address all correspondence to: sundg@cust.edu.cn

1 School of Science, Changchun University of Science and Technology, Changchun, China

2 Centre for Research in Photonics, University of Ottawa, Ottawa, ON, Canada

References

[1] Goos F, Hänchen HH. Ein neuer und fundamentalater versuch zur totalreflexion. Annals of Physics. 1947;**1**:333-346. DOI: 10.1002/andp.19474360704

[2] Artmann K. Berechnung der seitenversetzung des totalreflektierten strahles. Annals of Physics. 1948;**6**:87-102. DOI: 10.1002/andp.19484370108

[3] Chiu KW, Quinn JJ. On the Goos-Hänchen effect: A simple example of a time delay scattering process. American Journal of Physics. 1972;**40**:1847-1851. DOI: 10.1119/1.1987075

[4] Wild WJ, Giles CL. Goos-Hänchen shifts from absorbing media. Physics Review. 1982; **A25**:2099-2101. DOI: 10.1103/PhysRevA.25.2099

[5] Lai HM, Chen FC, Tang WK. Goos-Hänchen effect around and off the critical angle. Journal of the Optical Society of America. 1986;**A3**:550-557. DOI: 10.1364/JOSAA.3.000550

[6] Lai HM, Chan SW. Large and negative Goos-Hänchen shift near the Brewster dip on reflection from weakly absorbing media. Optics Letters. 2002;**27**:680-682. DOI: 10.1364/OL.27.000680

[7] Qing DK, Chen G. Goos-Hänchen shifts at the interfaces between left- and right-handed media. Optics Letters. 2004;**29**:872-874. DOI: 10.1364/OL.29.000872

[8] Oh GY, Kim DG, Choi YW. The characterization of GH shifts of surface plasmon resonance in a waveguide using the FDTD method. Optics Express. 2009;**17**:20714-20720. DOI: 10.1364/OE.17.020714

[9] Merano M, Aiello A, Exter MP, Woerdman JP. Observing angular deviations in the specular reflection of a light beam. Nature Photonics. 2009;**3**:337-340. DOI: 10.1038/NPHOTON.2009.75

[10] Ziauddin SQ, Quama S, Zubairy MS. Coherent control of the Goos-Hänchen shift. Physics Review. 2010;**A81**:023821. DOI: 10.1103/PhysRevA.81.023821

[11] Wang LG, Chen H, Zhu SY. Large and negative Goos-Hänchen shift near the Brewster dip on reflection from weakly absorbing media. Optics Letters. 2005;**30**:2936-2938

[12] Aiello A. Goos-Hänchen and Imbert-Fedorov shifts: A novel perspective. New Journal of Physics. 2012;**14**:1-12. DOI: 10.1088/1367-2630/14/1/013058

[13] Bliokh KY, Aiello A. Goos-Hänchen and Imbert-Fedorov beam shifts: An overview. Journal of Optics. 2013;**15**:014001. DOI: 10.1088/2040-8978/15/1/014001

[14] Rechtsman MC, Kartashov YV, Setzpfandt F, Trompeter FH, Torner L, Pertsch T, Peschel U, Szameit A. Negative Goos-Hänchen shift in periodic media. Optics Letters. 2011;**36**:4446-4448. DOI: 10.1364/OL.36.004446

[15] Steinberg AM, Chiao RY. Tunneling delay times in one and two dimensions. Physics Review. 1994;**A49**:3283-3295. DOI: 10.1103/PhysRevA.49.3283

[16] Sun DG. A proposal for digital electro-optic switches with free-carrier dispersion effect and Goos-Hanchen shift in silicon-on-insulator waveguide corner mirror. Journal of Applied Physics. 2013;**114**:104502. DOI: 10.1063/1.4820378

[17] Campenhout JV, Greens WMJ, Vlasov YA. Design of a digital, ultra-broadband electro-optic switch for reconfigurable optical networks-on-chip. Optics Express. 2009;**17**:23979-23808. DOI: 10.1364/OE.17.023793

[18] Reed GT, Mashanovich G, Gardes FY, Thomson DJ. Silicon optical modulators. Nature Photonics. 2010;**4**:518-526. DOI: 10.1038/nphoton.2010.179

[19] Sun DG, Liu P, Hall TJ. Realization for the high electro-optic modulation depth of silicon-on-insulator waveguide devices. In: Proceedings of the IEEE 2013 International Conference on Control Engineering and Information Technology (ICCIT2013); 9-11 August 2013; Nanning, China: IEEE; 2013. pp. 700-703

[20] Chan CC, Tamir T. Angular shift of a Gaussian beam reflected near the Brewster angle. Optics Letters. 1985;**10**:378-380. DOI: 10.1364/OL.10.000378

[21] Tamir T. Nonspecular phenomena in beam fields reflected by multilayered media. Journal of the Optical Society of America. 1986;**A3**:558-565. DOI: 10.1364/JOSAA.3.000558

[22] Aiello A, Merano M, Woerdman JP. Duality between spatial and angular shifts in optical reflection. Physics Review. 2009;**A88**:061801. DOI: 10.1103/PhysRevA.80.061801

[23] Bachmann M, Besse PA, Melchior H. General self-imaging properties in NN multimode interference couplers including phase relations. Applied Optics. 1994;**33**:3905-3911. DOI: 10.1364/AO.33.003905

[24] Soldano LB, Pennings ECM. Optical multimode interference devices based on self-imaging: Principles and applications. Journal of Lightwave Technology. 1995;**13**:615-627. DOI: 10.1109/50.372474

[25] Kawano K, Kitoh T. Schrödinger equation. In: Introduction to Optical Waveguide Analysis—Solving Maxwell's Equations and the Schrödinger Equation. New York, USA: Wiley Interscience; 1995. pp. 615-627. DOI: 10.1002/0471221600.ch7

[26] Himeno A, Terui H, Kobayashi M. Loss measurement and analysis of high-silica reflection bending waveguides. Journal of Lightwave Technology. 1998;**6**:41-46. DOI: 10.1109/50.396

[27] Sun DG, Li X, Wong D, Hu Y, Luo F, Hall TJ. Modeling and numerical analysis for silicon-on-insulator rib waveguide corner. Journal of Lightwave Technology. 2009;**27**:4610-4618. DOI: 10.1109/JLT.2009.2025609

IntechOpen